The cholesterol-binding motif of the HIV-1 glycoprotein gp41 regulates lateral sorting and oligomerization.

Roland Schwarzer[a], Ilya Levental[b], Andrea Gramatica[a], Silvia Scolari[a], Volker Buschmann[c], Michael Veit[d], and Andreas Herrmann[a,§]

[a] Department of Biology, Molecular Biophysics, Humboldt University Berlin, 10115 Berlin, Germany
[b] Laboratory of Membrane Biology, Department of Integrative Biology and Pharmacology, The University of Texas, 6431 Fannin Street, Houston, Texas 77030
[c] PicoQuant GmbH, 12489 Berlin, Germany
[d] Department of Immunology and Molecular Biology, Free University, Berlin, Germany

§ to whom correspondence should be addressed:
Andreas Herrmann
Humboldt Universität zu Berlin
Mathematisch-Naturwissenschaftliche Fakultät I
Institut für Biologie/Biophysik
Invalidenstraße 42
D-10115 Berlin
phone: +49-30-2093-8860
fax: +49-30-2093-8585
Email: andreas.herrmann@rz.hu-berlin.de

Abstract:

Enveloped viruses often use membrane lipid rafts to assemble and bud, augment infection and spread efficiently. However, the molecular bases and functional consequences of the partitioning of viral glycoproteins into microdomains remain intriguing questions in virus biology. Here, we measured Foerster Resonance Energy Transfer by Fluorescence Lifetime Imaging Microscopy (FLIM-FRET) to study the role of distinct membrane proximal regions of the human immunodeficiency virus glycoprotein gp41 for lipid raft partitioning in living Chinese hamster ovary cells (CHO-K1). Gp41 was labeled with a fluorescent protein at the exoplasmic face of the membrane, preventing any interference of the fluorophore with the proposed role of the transmembrane and cytoplasmic domains in lateral organization of gp41. Raft localization was deduced from interaction with an

established raft marker, a fluorescently tagged glycophosphatidylinositol anchor and the Cholesterol

Recognition Amino Acid Consensus (CRAC) was identified as the crucial lateral sorting determinant in

CHO-K1 cells. Interestingly, the raft association of gp41 indicates a substantial cell-to-cell

heterogeneity of the plasma membrane microdomains. In complementary fluorescence polarization

microscopy, a distinct CRAC requirement was found for the oligomerization of the gp41 variants. Our

data provide further insight into the molecular basis and biological implications of the cholesterol

dependent lateral sorting of viral glycoproteins for virus assembly at cellular membranes.

Introduction:

The envelope protein (Env) is the only membrane spanning and surface exposed protein of HIV-1. It plays a crucial role in the viral replication cycle by mediating host cell binding and fusion between cellular and viral membrane required for releasing the viral genome into the host cell. The functional form of the Env spikes is composed of trimers of non-covalent gp120/gp41 heterodimers. Whereas the surface subunit gp120 initiates cell infection by binding the primary receptor CD4 and the coreceptor CCR5 or CXCR4, the transmembrane subunit gp41 promotes membrane fusion by inserting into the target membrane and triggering the fusion reaction (Wyatt and Sodroski, 1998).

Although much is known about the relevance and function of Env in virus entry, many questions remain regarding its incorporation into assembling virus particles. The envelope complex is initially synthesized as a precursor with a molecular mass of 160 kDa in the endoplasmic reticulum (ER) of the infected cell. After N-glycosylation and chaperone assisted folding, gp160 trimerizes and is transferred to the Golgi apparatus. Here, carbohydrates are processed and the protein is endoproteolytically cleaved into two subunits (Earl *et al.*, 1991). Although this cleavage decreases oligomer stability (Earl *et al.*, 1990), the complex remains assembled as a trimer of gp120/gp41 heterodimers that is finally transported to the plasma membrane, the site of assembly and budding of HIV-1. However, Env is efficiently re-internalized from the cell surface by endogenous endocytic machinery (Rowell *et al.*, 1995; Ohno *et al.*, 1996; Ohno *et al.*, 1997). This trafficking appears counter-productive for viral assembly, but it seems to be functionally advantageous for the virus, since gp41 harbors several highly conserved cytoplasmic endocytosis signals (Gao *et al.*, 1996). It has been surmised that this re-internalization minimizes exposure of the viral gp41 to the immune system (Yuste *et al.*, 2005; Veillette *et al.*, 2013) as well as mitigating cell lytic effects of plasma membrane residing gp41 (Sodroski *et al.*, 1986; Lifson *et al.*, 1986; Somasundaran and Robinson, 1987; Koga *et al.*, 1991).

3

In recent years, compelling evidence points to an important role for cholesterol enriched, ordered lipid and protein microdomains – often called lipid rafts – in HIV-1 assembly (Dubay *et al.*, 1992; Aloia *et al.*, 1993; Yu *et al.*, 1993; Nguyen and Hildreth, 2000; Mañes *et al.*, 2000; Rousso *et al.*, 2000; Chen *et al.*, 2001; Ono and Freed, 2001; Popik *et al.*, 2002; Stephen Campbell *et al.*, 2002; Guyader *et al.*, 2002; Liao *et al.*, 2003; Graham *et al.*, 2003; Bhattacharya *et al.*, 2004; Campbell *et al.*, 2004; Chan *et al.*, 2005; Bhattacharya *et al.*, 2006). If such domains are sites of aggregation of viral proteins and virion assembly, gp41 should be preferentially sorted to lipid rafts in cellular membranes. However, the molecular basis of this putative raft partitioning remains under debate. To date, most attention has been devoted to the gp41 cytoplasmic tail and it was demonstrated recently, that this part is responsible for large accumulations of the protein at the HIV-1 assembly site (Muranyi *et al.*, 2013; Roy *et al.*, 2013). In absence of other viral components however, the proteins was found to be excluded from large clusters but remains heterogeneously distributed in small clusters in a cytoplasmic tail independent manner (Muranyi *et al.*, 2013; Roy *et al.*, 2013). Distinct motifs, such as the membrane interacting lentivirus lytic peptides or specific cytoplasmic cysteines of gp41 which are known targets for palmitoylation have been reported to be responsible for the Gag-independent lateral sorting in plasma membrane lipid rafts (Zacharias *et al.*, 2002; Resh, 2006; Epand, 2008; Scolari *et al.*, 2009; Yang *et al.*, 2010; Leventhal, Grzybek, *et al.*, 2010; Leventhal, Lingwood, *et al.*, 2010). Another potentially relevant motif for lateral segregation of proteins in the plasma membrane is the Cholesterol Recognition Amino Acid Consensus (CRAC) (Vincent *et al.*, 2002; Bhattacharya *et al.*, 2004; Epand and Thomas, 2006; Chen *et al.*, 2009). The gp41 CRAC domain is embedded in the nonpolar part of the Membrane Proximal External Region (MPER), an amphiphilic α-helix of the ectodomain adjacent to the gp41 transmembrane domain (TMD) which could be demonstrated to specifically bind cholesterol (Vincent *et al.*, 2002). Moreover, this sequence motif is highly conserved (LWY 99%, LWYI 98%, LWYIK 76%, LWYIR 21%, see Experimental Procedures for details) and mutations of single amino acids were shown to significantly reduce virus replication (Salzwedel *et al.*, 1999).

4

In this study we have investigated structural determinants of gp41 cellular organization, in particular the roles of the cytoplasmic tail, the TMD, and the MPER motif in the association of gp41 with lipid rafts in the plasma membrane and Golgi apparatus of living CHO-K1 cells. Fluorescence Lifetime Imaging Microscopy (FLIM) was used to determine distance dependent Foerster Resonance Energy Transfer (FRET) between the well characterized, raft localized glycosylphosphatidylinositol anchored cyan fluorescent protein (GPI-CFP) (Zacharias et al., 2002; Sharma et al., 2004; Scolari et al., 2009) and gp41. The latter was tagged by replacing the N-terminal part of the gp41 ectodomain with a yellow fluorescent protein (gp41-YFP). If gp41-YFP, serving as FRET acceptor, associates with lipid rafts it should encounter the FRET donor, GPI-CFP with a high probability resulting in specific FRET (Zacharias et al., 2002; Scolari et al., 2009). As the protein's membrane associated sequences were left unchanged, the fluorescent probe within the gp41 constructs is unlikely to interfere with the role of these sequences, in particular cytoplasmic tail and transmembrane domain, in sorting and lateral membrane organization. In addition, to study the relevance of those domains for gp41-YFP oligomerization in live cells, we applied fluorescence anisotropy microscopy to measure homo-FRET which is reflective of oligomerization of YFP-labeled fusion proteins.

Results:

The lipid raft hypothesis (Simons and Ikonen, 1997) postulates the existence of dynamic, submicrometric, lateral domains in cellular membranes. We used the FLIM-FRET approach as recently described by us (Scolari et al., 2009) to elucidate the raft association of a protein in living cells. To this end, most of the gp41 ectodomain was substituted with a yellow fluorescent protein (YFP) (Fig. 1A and B) and upon coexpression with a GPI-anchored CFP, FRET was used as a reporter for enrichment of gp41-YFP in plasma membrane microdomains (see Supplementary Fig. S1 for proof of principle). To elucidate which parts of gp41 are responsible for the protein's raft association, four additional gp41 constructs were created (Fig. 1B). We removed most of the cytosolic domain by

5

conducting a truncation at amino acid 703 (construct Δ1) or the cytosolic domain and the membrane proximal external region by truncating at amino acid 703 and 670 (construct Δ2). Furthermore, a leucine to isoleucine single residue mutation, reported to reduce cholesterol affinity (Epand and Thomas, 2006), was introduced at position 670 in gp41 (gp41mCRAC) and at the corresponding position of Δ1 (Δ1mCRAC) to disrupt the CRAC domain. A GPI-anchored YFP construct, homologous to GPI-CFP was used as a raft residing FLIM-FRET positive control and a negative control for oligomerization.

The gp41 cytoplasmic tail controls subcellular distribution. To study the plasma membrane expression of the different fusion proteins, CHO-K1 cells were transfected with GPI-CFP, in this context primarily serving as plasma membrane marker, and the respective YFP-labeled construct. As expected (Sharma *et al.*, 2004; Scolari *et al.*, 2009), GPI-anchored proteins were mostly found at the plasma membrane with a perinuclear accumulation (Fig. 1C, Supplementary Fig. S1A) in less than half of the cells (40±4%; mean±SEM, n=6). In contrast the constructs gp41-YFP and gp41mCRAC showed strong accumulation in the perinuclear region in most of the cells (76±5% and 71±3%; mean±SEM, n=5 and n=4) and only a rather low occurrence at the plasma membrane (Fig. 1C, Supplementary Fig. S1A). The three cytoplasmic tail truncation variants, Δ1, Δ1mCRAC and Δ2, on the other hand were enriched in the plasma membrane with less frequent (63±8%, 60±11% and 68±2%; mean±SEM, n=5, n=3 and n=5) perinuclear accumulations (Fig. 1C).

To quantify the surface expression level, microscope images were analyzed using ImageJ. CFP images were used to select the plasma membranes since GPI-CFP was predominantly localized at the surface of the cells. Subsequently, the YFP-fluorescence intensity was measured in the same region of interest to obtain the plasma membrane expression of the YFP-labeled proteins. The highest surface exposure was expectedly found for GPI-YFP (Fig. 1D), whereas it was lower for the variant gp41-YFP. Both CRAC mutants, gp41mCRAC and Δ1mCRAC, showed comparable plasma membrane concentrations as their respective wildtype proteins gp41-YFP and Δ1 (Fig. 1D). Although Δ2 and Δ1

6

are enriched in the plasma membrane (see above), the surface exposure of Δ2 is much lower than that of Δ1 (Fig. 1D), most likely as a result of an overall lower expression.

The total expression of the different constructs cannot be expected to be similar and the cellular distribution has to be characterized to obtain reliable data regarding trafficking and re-internalization. To this aim, live cell flow cytometry experiments were conducted (Fig. 1E). Cells transfected with our YFP-tagged constructs were stained with anti-GFP fluorescent antibodies to quantify the amount of surface exposed proteins. The ratio of anti-GFP antibody to YFP signal was taken as a measure of plasma membrane to overall expression. In this assay, all variants with a truncated cytoplasmic tail, Δ1, Δ1mCRAC and Δ2 displayed similar ratios (Fig. 1E), whereas a significantly lower ratio was found for gp41-YFP and gp41mCRAC (Fig. 1E). This finding demonstrates that the cellular distribution is mainly controlled by the cytoplasmic tail since all truncation variants are deficient in the interactions with cellular adaptor proteins. The ectodomain, on the other hand that is removed in Δ2, did obviously not contribute to this property. In agreement with the microscope assay, both CRAC mutants displayed an intracellular distribution that resembles their respective wild type forms (Fig. 1E).

Gp41 constructs are palmitoylated. Gp41, like many other fusion-mediating glycoproteins of enveloped viruses, is S-acylated (specifically palmitoylated) by a saturated fatty acid (Yang *et al.*, 1995; Veit, 2012). Palmitoylation of proteins has been reported to play an essential role in raft targeting (Leventhal, Lingwood, *et al.*, 2010; Veit, 2012). Therefore, a biochemical assay was performed to verify palmitoylation of our gp41 constructs (Fig. 1F). Four different variants were tested using an acyl-biotinyl-exchange approach (Wan *et al.*, 2007), the wild type like variant gp41-YFP, its CRAC mutant gp41mCRAC, a palmitoylation mutant of gp41-YFP (C764A) and the truncation variant Δ1. Both constructs comprising the cytoplasmic tail, were found to be efficiently palmitoylated, whereas the palmitoylation mutant gp41mPalm and the truncation construct Δ1, which is lacking the acylation site, were not (Fig. 1F).

7

Gp41 partitions to lipid rafts in the plasma membrane. To assess lipid raft partitioning in live cells, FLIM experiments were conducted (Fig. 2A, for additional controls see Supplementary Fig. S1). Initially, CHO-K1 cells transfected with a GPI-CFP were examined with a confocal FLIM-FRET setup. Amplitude weighted fluorescence lifetimes of around 2.5 ns were obtained upon analysis of the plasma membrane (Fig. 2B). Different controls were performed to prove the reliability of the method. GPI-CFP was cotransfected with GPI-YFP as a raft clustering positive control (Fig. 2B). The proteins were found to be colocalized (Supplementary Fig. S1A) and a reduced average CFP lifetime at the plasma membrane was assessed, corresponding to a FRET efficiency of around 8% (Fig. 2B). For comparison, for a GPI-anchored construct with a linked CFP and YFP tag (Supplementary Fig. S1A) a FRET efficiency of around 20% was obtained. This can be considered as the upper limit of the efficiency between CFP and YFP in our assay (Fig. 2B).

As shown before, the intracellular distribution of the chimeric gp41-YFP differed from that of GPI-anchored fluorescent proteins. The construct was enriched in the perinuclear region and intracellular vesicles, with a smaller fraction at the plasma membrane (Fig. 1C, 2A, 2D; see also Supplementary Fig. S1A, S2 and S3). Nevertheless, upon coexpression the lifetime of GPI-CFP at the plasma membrane was significantly reduced, denoting FRET of around 5-6% (Fig. 2B). To exclude that this decrease of the CFP lifetime results from cellular changes induced by the overexpression of the viral protein, GPI-CFP cotransfected with gp41-cherry was investigated. Since the spectral overlap of cherry with CFP is insignificant in comparison to YFP and CFP, the donor lifetime reduction (hence FRET) in the presence of this acceptor fluorophore should be less pronounced. Indeed, essentially no decrease in the CFP fluorescence lifetime (Fig. 2B) was observed, confirming that the lifetime reduction in the presence of YFP labeled fusion proteins is a result of intermolecular FRET.

The extracellular CRAC motif is crucial for gp41 plasma membrane raft association. The truncation variant Δ1 was found to be enriched at the plasma membrane compared to gp41-YFP and Δ2 (Fig. 1C,

8

D). Nevertheless, cotransfection of gp41-YFP, Δ1 or Δ2 with the raft marker GPI-CFP caused comparable decreases of donor lifetimes at the plasma membrane with no statistically relevant differences in the FRET efficiency (Fig. 2C). Since the plasma membrane expression significantly differs between the gp41 variants, this finding indicates that FRET efficiency is fairly concentration-independent in the range relevant for our experiments. Furthermore, this result demonstrates that neither one of the cytosolic membrane interacting factors, namely lentivirus lytic peptides or palmitoylation sites, nor the amphipathic membrane proximal external region are mandatory for gp41 raft association.

To investigate the role of the cholesterol binding motif in the gp41 lateral organization, CRAC mutants of gp41-YFP and the variant Δ1 were examined. Upon cotransfection with GPI-CFP, significantly lower FRET efficiencies were found for both, gp41mCRAC and Δ1mCRAC (Fig. 2C). Since intracellular distribution and expression levels of the mutants were comparable to their respective wild type (Fig. 1D, E) this finding implicates a specific role for the CRAC motif in sorting gp41 to lipid rafts domains containing GPI-anchored protein.

CRAC-dependent raft association of gp41 already occurs in the Golgi apparatus. For all fluorescently labeled proteins used in this study, accumulations in perinuclear regions were observed. To clearly identify this cellular compartment, antibody based staining was conducted with gp41-YFP expressed in CHO-K1 cells and the Golgi apparatus stained with anti-58K or anti-Giantin antibodies. Both cellular, Golgi residing proteins (Schweizer *et al.*, 1988; Linstedt *et al.*, 1995) clearly colocalized with the gp41-YFP in the perinuclear region (Fig. 2D) demonstrating that this intracellular protein accumulation site indeed constitutes the Golgi compartment.

It has been hypothesized that lipid rafts, which are generally supposed to be a feature of plasma membranes (Owen *et al.*, 2012), already emerge in the Golgi apparatus and exocytic vesicles (Shahan M Campbell *et al.*, 2002; Resh, 2004; Vetrivel *et al.*, 2004; Simons and Sampaio, 2011; Surma *et al.*, 2012). Therefore, we also analyzed FLIM-FRET in the perinuclear region. In our experimental setup

9

FRET is assessed as changes of the fluorescence lifetime of the FRET-donor GPI-CFP. However, only a small fraction of GPI-CFP expressing cells showed a signal in the Golgi-apparatus and therefore only a limited number could be analyzed. Notably, even in the absence of acceptor, the lifetime of GPI-CFP was lower in the Golgi apparatus than at the plasma membrane (Fig. 2A). Different reasons may account for the latter: CFP lifetimes depend on different parameters, such as for example pH (Villoing *et al.*, 2008) or ATP concentration (Borst *et al.*, 2010) that significantly differ between Golgi lumen and extracellular environment (Thompson *et al.*, 2006; Rivinoja *et al.*, 2009). Nevertheless, FLIM-FRET between GPI-CFP and all gp41 variants was assessed and the differences observed at the PM were also found in the Golgi. Again, all CRAC containing gp41-chimera showed robust FRET (Fig. 2E), with lower FRET for both CRAC mutants (Fig. 2E). This finding supports the previous observation of a CRAC dependent raft partitioning. Moreover, the fact that FRET efficiencies in this perinuclear region are similar to the plasma membrane values points to a lateral segregation already in the Golgi-apparatus. However, statistically significant differences between wildtype and CRAC mutant were only found for gp41-YFP but not for Δ1 (Fig. 2E). This might be a result of the rather high variance of the values and the limited number of available cells showing Golgi localization of the respective constructs.

Clustering analysis supports raft partitioning of CRAC-containing gp41 variants. To verify the reliability of our FLIM-FRET approach we used a model introduced by Zacharias et al. (Zacharias *et al.*, 2002). The underlying hyperbolic function describes a simple saturable binding that possesses two free parameters, the saturation level and the dissociation constant K_d that represents the raft affinity of the protein under study. The model assumes that, if energy transfer only originates from random interactions of fluorophores diffusing freely in the membrane, there should be a linear dependence of FRET on the acceptor concentration and therefore high FRET values should be only achieved with very high acceptor concentrations. In contrast, specific interaction or co-recruitment into lateral domains should yield FRET efficiencies that are essentially independent of acceptor concentrations with a saturation of energy transfer even at low concentrations of the acceptor. We tested this

10

dependence by plotting the plasma membrane acceptor intensity versus the respective FRET efficiency for at least 20 cells per gp41 construct (Fig. 3A). FRET efficiencies of cells expressing the CRAC containing variants (gp41-YFP and Δ1) showed saturation at low expression levels (Fig. 3A), indicating specific association in membrane microdomains rather than concentration dependent, random interactions within the lipid bilayer. In contrast, the dependence of FRET on acceptor intensity for the CRAC mutants (gp41mCRAC and Δ1mCRAC) does not allow to conclude whether it is proportional to the PM concentration of the protein or it shows a weak saturation behavior. In any case, the FRET values even for high acceptor intensity are much lower in comparison to that of the CRAC containing variants. Since expression and intracellular localization of the wildtype forms and CRAC mutants are similar (Fig. 1D, E), this difference clearly demonstrate CRAC dependent lateral arrangement of the glycoprotein (see Supplementary Fig. S4 for the Δ2 construct).

Importantly, the distribution of experimentally observed FRET values for gp41-YFP and Δ1 (Fig. 3) suggests an additional complexity of the studied system. Although the values of CRAC containing variants do clearly show FRET saturation at low expression levels, fitting according to the model of Zacharias et al. does not provide an appropriate description of the data. Rather, the plot suggests a heterogeneous distribution of FRET values which may suggest different populations of cells and we found a similar distribution of FRET values for all three CRAC containing constructs in the clustering analysis (Fig. 3A: gp41-YFP, Δ1; for Δ2 see Supplementary Fig. S4). Therefore, to shed further light on cell-to-cell differences, we pooled FRET data of gp41-YFP, Δ1 and Δ2 in one histogram (Fig. 3B) obtaining a more accurate analysis due to the high number of observations considered. We found a bimodal distribution with peaks at 6 and 18% FRET efficiency, comprising about 80 and 20%, respectively, of all cells measured. This observation points towards significant deviations of the plasma membrane organization between individuals of a cell line population (see Discussion).

Gp41 oligomerization is CRAC dependent. In recent years, several determinants of gp41 oligomerization have been reported. The transmembrane domain (Lenz *et al.*, 2005; Kim *et al.*, 2009)

and extracellular region (Poumbourios *et al.*, 1995; Bernstein *et al.*, 1995; Center *et al.*, 1997; McInerney *et al.*, 1998; Liu and Lu, 2010; Liu *et al.*, 2010), but also the gp41 cytoplasmic tail (Yang *et al.*, 2010) were shown to be involved in trimer assembly. However, the constructs in our study lack a considerable portion of the external region of gp41 and the complete gp120 interaction partner. To elucidate which of the remaining protein domains might be relevant for oligomerization, the different gp41 truncation and mutation variants were compared by conducting fluorescence anisotropy measurements (Scolari *et al.*, 2009). This approach is based on the fact that oligomerization of fluorescently labeled protein induces homo-FRET and this energy migration directly influences the anisotropy of the respective fluorescence. Typically, low anisotropy values report oligomerization whereas higher values are indicative of monomers.

A homogeneous and localization independent fluorescence anisotropy of about 0.3 was found (Fig. 4) for the GPI-YFP construct serving as a oligomerization negative control. This is in agreement with previous results (Sharma *et al.*, 2004; Scolari *et al.*, 2009) and indicative of a lipid raft clustered, monomeric protein (Sharma *et al.*, 2004). Next, gp41-derived chimeras were analyzed. As expected, upon averaging of the anisotropy values of several individual cells, low anisotropy values of around 0.2 were found for gp41-YFP and Δ1 expression (Fig. 4A, B). In contrast, anisotropy values comparable to the monomeric control GPI-YFP were obtained for both CRAC-mutants, gp41mCRAC and Δ1mCRAC and the truncation variant Δ2 (Fig. 4A, B).

Notably, the variant Δ1 showed a localization-dependent oligomerization (Fig. 4A, C). While a high fluorescence anisotropy above 0.2 was found in all intracellular compartments, including Golgi apparatus and ER, a significant decrease down to 0.1 was found at the plasma membrane (Fig. 4C). This decrease of fluorescence anisotropy again is indicative of oligomerization of the Δ1 variant (see Supplementary Fig. S4). Hence, this observation reports that Δ1 oligomers were predominantly found at the plasma membrane and suggests that their assembly largely occurs at the cell surface and not in intracellular membranes. In contrast, gp41-YFP was not only found to be oligomeric at the plasma membrane but also in intracellular membrane compartments (Fig. 4C).

12

Discussion:

We have investigated the lateral organization of the HIV-1 glycoprotein gp41 and the determinants of targeting to specific lipid microenvironments by a live cell imaging approach. Because numerous previous studies have indicated that the glycoprotein's cytoplasmic tail is important for gp41 cellular organization (Rousso *et al.*, 2000; Wyss *et al.*, 2001; Bhattacharya *et al.*, 2004; Lopez-Vergès *et al.*, 2006; Byland *et al.*, 2007; Yang *et al.*, 2010), we replaced the N-terminal part of the gp41 ectodomain with YFP to avoid any influence of the label on a potential function of the internal domain. Truncation and mutation variants were assessed for their interaction with the well-established raft marker GPI-CFP (Zacharias *et al.*, 2002; Sharma *et al.*, 2004; Scolari *et al.*, 2009) by FLIM-FRET. Since FRET efficiencies in this assay depend on many different parameter (average lipid raft size, donor and acceptor concentration and orientation to each other, lipid raft affinity of GPI-anchored proteins and gp41-YFP) the assessed data allow only a semi-quantitative analysis of the gp41 raft partitioning.

The FLIM-FRET approach was complemented by fluorescence anisotropy imaging microscopy, flow cytometry and confocal microscopy to study oligomerization and plasma membrane expression of the different variants. CHO-K1 cells were applied since they do not only represent one of the most commonly used cells lines but have also been intensively investigated with respect to lateral plasma membrane organization and lipid rafts (Varma and Mayor, 1998; Mukherjee *et al.*, 1998; Mañes *et al.*, 2000; Zheng *et al.*, 2001; Sugimoto *et al.*, 2001; Zheng *et al.*, 2003; Sharma *et al.*, 2004; Silvius, 2005; Silvius and Nabi, 2006; Kellner *et al.*, 2007; Scolari *et al.*, 2009; Engel *et al.*, 2010; Sanchez *et al.*, 2012), which are the focus of this study.

We have made two major observations. First, the CRAC domain is the main determinant for the enrichment of gp41 in raft domains of the plasma membrane and Golgi apparatus. Secondly, the gp41 constructs oligomerizes in the plasma membrane depending on the presence of the CRAC

13

domain. Intracellular oligomer abundance was found to require the cytoplasmic tail whereas plasma

membrane oligomerization was independent of the tail but required factors of the ectodomain.

Surface exposure of gp41 constructs. To address the impact of the mutation and truncations on the

intracellular distribution of the protein, two independent assays were conducted. Plasma membrane

exposure of our gp41 variants depends on the cytoplasmic tail. The surface expression relative to the

whole cells increased around 2 to 3 fold upon truncation of the tail. This observation is in agreement

with previous publications reporting restriction of the plasma membrane localization of Env by motifs

of the tail enabling interaction with cytoplasmic adaptor proteins that cause clathrin-mediated

endocytosis (Ohno *et al.*, 1997; Berlioz-Torrent *et al.*, 1999; Wyss *et al.*, 2001; Day *et al.*, 2006; Byland

et al., 2007). However, mutation of the CRAC domain did not influence the intracellular distribution

and plasma membrane surface exposure.

Gp41 raft partitioning. We measured gp41-YFP partitioning into plasma membrane lipid rafts by

demonstrating colocalization with GPI-CFP on nanometer scale utilizing FRET. Neither abolishing of

the protein's cytosolic domain, nor the additional removal of the remaining gp41 external region

significantly impaired this lateral segregation behavior. On the other hand, a single amino acid

change in the CRAC domain decreased the average FRET efficiency, hence microdomain association,

of two different gp41 constructs. Considering the robust raft partitioning of the minimal variant (Δ2),

these results demonstrate that the CRAC is a sufficient determinant of the raft association of gp41-

YFP. Other motifs like the palmitoylated cysteine residues or amphipathic α-helices, proposed to

influence lateral plasma membrane sorting (Zacharias *et al.*, 2002; Resh, 2006; Epand, 2008; Scolari

et al., 2009; Yang *et al.*, 2010; Leventhal, Grzybek, *et al.*, 2010; Leventhal, Lingwood, *et al.*, 2010), do

not contribute measurably to this property of our gp41 constructs in CHO-K1 cells.

Although compelling experimental data points to an important function of lipid rafts for HIV

assembly (Brügger *et al.*, 2006), previous studies regarding intrinsic Env features that mediate lateral

14

sorting reported inconsistent findings. Whereas gp41 CRAC peptides were clearly shown to specifically bind cholesterol (Vincent *et al.*, 2002), mutations of the CRAC domain did not interfere with the sequestering of gp41 in detergent resistant membrane fractions (Chen *et al.*, 2009). The role of gp41 acylation in this context is even more unclear and at least partly contradictory (Rousso *et al.*, 2000; Chan *et al.*, 2005). What is the reason for these inconsistencies? Our results reflect the lateral sorting behavior of the proteins under study in a native and undisturbed environment of living cells (see Supplementary Fig. S6). Many previous investigations of gp41 raft association were based on DRM assays, which are highly controversial, and potentially prone to artifacts (Lichtenberg *et al.*, 2005). In general, results from those methods may not reflect physiological conditions and have to be taken with care. Another source of inconsistent observations could be differences of the gp41 sequences between used HIV-1 isolates. However it is striking that screenings of gp41 genetic diversity revealed a high conservation of the protein's cholesterol binding motif while palmitoylated cysteine residues turned out to be more variable (Gao *et al.*, 1996). This observation argues against palmitoylations as a prerequisite for efficient virus assembly and supports the hypothesis that CRAC is the key factor of lateral gp41 sorting.

It is of note that our results are highly consistent with recently published works based on a direct visualization of Gag and Env clustering using super resolution microscopy (Muranyi *et al.*, 2013; Roy *et al.*, 2013). In those studies, lateral accumulation of Env was shown in the plasma membrane of different mammalian cells and it was found to be significantly enlarged in the presence of Gag. Nevertheless, clustering of Env was even found in absence of Gag, and a cytoplasmic tail deficient variant did not show significant differences in the cluster size compared to the wildtype. This finding supports our conclusion of plasma membrane raft partitioning independent of the gp41 cytosolic domain and thus palmitoylation.

Our FLIM-FRET data for gp41-YFP, Δ1, and Δ2 point to at least two populations of cells with respect to their FRET efficiencies. This observation suggests the existence of heterogeneities in the cell population that result in a cell-to-cell variability of plasma membrane lipid and protein organization.

15

We hypothesize that this could originate from different lipid rafts existing in plasma membranes of the respective cells. Indeed, light and heavy rafts have already been described, possessing different densities in sucrose gradients and being enriched in different proteins (Nebl *et al.*, 2002; Bhattacharya *et al.*, 2004). However, whether this finding reflects cellular changes within the cell cycle or are a result of other local parameters like for example specific position of a cell in a colony, cell density or other causes (Snijder *et al.*, 2009) needs to be studied further. In general, our observation underlines the relevance of single-cell experiments, but also the importance of analyzing a high number of individual cells in those assays. In our approach, many (typically 50 up to several hundred) randomly selected cells were examined to ensure that average FRET efficiencies represent individuals from all cell populations for all proteins studied.

Gp41 oligomerization. The question remains, what is the biological relevance of gp41 raft localization. Why is a conservation of a cholesterol binding motif beneficial for human immunodeficiency viruses? A prevalent answer is a common local enrichment of the virus components in lipid rafts to facilitate the virus assembly. Indeed, a decrease in virus particle production upon cholesterol depletion has been observed (Ono and Freed, 2001). Yet, another hypothesis could be derived from our study on oligomerization of gp41 constructs.

We show that gp41-YFP, even in the absence of gp120 and a significant part of the gp41 ectodomain, has the propensity to form oligomers. In contrast to previous, indirect studies on full length gp41 (Lenz *et al.*, 2005; Kim *et al.*, 2009) we demonstrated, that the transmembrane domain of gp41 is not sufficient for efficient oligomer assembly. Moreover, we found that oligomerization of the gp41-YFP construct is diminished for variants with CRAC mutations or truncations of the gp41 ectodomain. Those observations confirm studies reporting MPER and adjacent heptad region to be involved in the trimerization (Poumbourios *et al.*, 1995; Bernstein *et al.*, 1995; Center *et al.*, 1997; McInerney *et al.*, 1998; Liu and Lu, 2010; Liu *et al.*, 2010) but in addition implicate a function of the CRAC domain for efficient assembly - or at least stabilization of protein oligomers. Possibly, the importance of the

16

CRAC domain for oligomerization may suggest that oligomers are preferentially formed and stabilized in microdomains, in particular in the late Golgi apparatus and at the plasma membrane.

What could be the relevance of this CRAC dependent oligomerization of the gp41-YFP construct? It is well known that gp160 (gp41/gp120) trimerizes in the ER (Earl *et al.*, 1990; Checkley *et al.*, 2011). After enzymatic cleavage of the precursor gp160 in the Golgi apparatus both subunits remain associated by weak, noncovalent interactions but the stability of the trimer is significantly reduced (Earl *et al.*, 1990). However, the emerging local enrichment of the glycoproteins in lipid rafts of the Golgi apparatus and later in the plasma membrane might compensate for this destabilization. Thus, lipid rafts may not only serve as platforms for protein enrichment but also as structures that stabilize protein complexes.

In conclusion, our study demonstrates that the membrane adjacent parts of gp41, i.e. the cytoplasmic tail, the MPER, and most notably the CRAC domain have intrinsic properties promoting lipid raft partitioning, oligomer abundance and stability but also surface exposure of the protein (summarized in Table 1). In particular, the importance of the CRAC domain for lateral sorting and oligomerization has often been underestimated and requires further investigations. It is conceivable that this crucial sequence can provide a target to counteract HIV infection or spread in the future.

Experimental procedures:

Gp41 and raft marker constructs. As raft marker protein, the GPI-anchored Cyan Fluorescent Protein initially provided by Patrick Keller (Keller *et al.*, 2001) and an analogous Yellow Fluorescent Protein labeled variant was used in its monomeric form (A206K) as described in Scolari et al. (Scolari *et al.*, 2009). To generate gp41 fusion proteins, a trafficking signal peptide was linked to the N-terminus of the pEYFP-N1 vector YFP and the A206K mutation was introduced, to prevent fluorophore dimerization. Parts of the HIV-1 JRFL-envelope isolate (uniprotentry: Q75760) were then fused to the

17

C-terminus of the fluorophore resulting in fluorescently labeled membrane proteins. Based on predicted structures of the glycoprotein (Abad *et al.*, 2009), an amino acid sequence was selected, containing all parts that have been supposed to interact with the membrane. The protein has the following amino acid sequence $_{625}$EIDNY TSEIYTLIEE SQNQQEKNEQ ELLELDKWAS LWNWFDITKW LWYIKIFIMI VGGLVGLRLV FTVLSIVNRV RQGYSPLSFQ TLLPAPRGPD RPEGIEEEGG ERDRD RSGRL VNGFLALIWV DLRSLCLFSY HRLRDLLLTV TRIVELLGRR GWEVLKYWWN LLQYWSQELK NSAVSLLNAT AIAVAEGTDR IIEALQRTYR AILHIPTRIR QGLERALL$_{847}$ with the transmembrane domain underlined. The additional variants of this protein, produced by introducing different truncations and mutations are described in detail in the results section.

Treatment of cells. Chinese Hamster Ovary (CHO-K1) cells were maintained in Dulbecco's modified Eagle medium (DMEM, PAA Laboratories GmbH, Austria) containing 10% fetal bovine serum. 24 h prior to experiments, fusion protein expression plasmids were transfected into CHO cells in 35-mm-diameter plates utilizing Lipofectamine (Invitrogen, Carlsbad, CA) according to the manufacturer protocol.

Quantitative membrane expression experiments. To assess quantitative information about the relative plasma membrane expression of fusion protein, confocal images were analyzed using ImageJ. Assuming a direct proportion between acceptor concentration and fluorescence signal, normalized and background corrected YFP fluorescence at the plasma membrane were obtained for every protein from 20-50 cells measured in at least 3 independent experiments.

Cell cytometer membrane expression experiments. CHO cells were first transfected with fusion proteins for 24 h, detached using PBS/EDTA (5mM) and then incubated with AlexaFluor594-labeled anti–GFP FA as described before for 60 min at 4°C. Then, cells were washed, spun down (200g, 10min) and resuspended in PBS. In cytometer experiments, the YFP positive population was selected

18

and the average FA signal of the respective cells was assumed as a direct reporter of YFP plasma membrane localization during the labeling period. 2 independent experiments were performed for each protein.

Acyl-biotinyl exchange. Acyl-biotinyl exchange was performed as described by Wan et al. (Wan *et al.*, 2007) to qualitatively asssess palmitoylation of gp41 variants. Briefly, chemical exchange of thioester-linked protein acyl modifications for a thiol-reactive, reducible biotin probe allows specific enrichment of palmitoylated proteins by affinity pulldown with streptavidin-coated beads. Gp41 variants were identified in pull-down (i.e. palmitoylated) and input fractions by Western blotting with anti-GFP antibodies (Roche, Mannheim, Germany).

Confocal and FLIM-FRET imaging. An inverted FluoView 1000 microscope (Olympus, Tokyo, Japan) was modified for FLIM-FRET measurements with a time-resolved LSM Upgrade kit (PicoQuant, Berlin, Germany). Differential Interference Contrast (DIC), fluorescence intensity and FLIM images were obtained with a 60x oil immersion objective (numerical aperture 1.35) at 25°C with a frame size of 512 x 512 pixels. For confocal imaging, CFP was excited at 458 nm using a laser diode and observed in 475 to 490 nm detection range. YFP was excited at 515 nm using an argon laser and detected in the range of 535 to 575 nm. YFP and CFP signals of coexpressing cells were recorded sequentially and obtained intensities were analyzed with the ImageJ analysis program. Cherry and Alexa594 constructs were exited at 559 nm using a laser diode and detected between 570 and 670 nm. For FLIM measurements, CFP was excited with a pulsed 440 nm laser diode with a 20 MHz pulse frequency and detected using a τ single photon avalanche photodiode (τ-SPAD, PicoQuant) equipped with a 470/30 bandpass filter. SPAD signals were processed with the TimeHarp 300 photon counting board and analyzed with the SymPhoTime software (PicoQuant) taking into account the instrument response function to allow consideration of short lifetime components with a high accuracy. FLIM images were acquired as described previously (Scolari *et al.*, 2009). Briefly, images were accumulated

for 98 s with an average photon count rate of 40000-60000 counts per second. Regions of interest were selected from FLIM images and time-resolved photon-counts were summed up into a lifetime histogram within the SymPhoTime software. The intensity distribution decay was further analyzed by fitting using a nonlinear least squares iterative procedure as the sum of 2 exponential terms. As other fluorescent protein variants, CFP adopts 2 different conformational states (Seifert *et al.*, 2002; Hyun Bae *et al.*, 2003) with different fluorescence properties that have to be considered in fluorescence lifetime fits. For every single cell the amplitude weighted average lifetime was calculated according to

$$\tau_{AV} = \frac{\sum_i \alpha_i \tau_i}{\sum_i \alpha_i}$$

Where τ_{av} is the amplitude average weighted lifetime, α is the amplitude of a lifetime component and τ is the corresponding lifetime. FLIM images were generated by the SymPhoTime software by displaying pixel-wise average lifetimes in pseudocolors.

The calculated decays were judged by the χ^2 values and the residuals of the fit. To quantify occurring FRET, cells expressing donor protein alone or coexpressing donor and FRET-acceptor protein were measured and the FRET efficiency was calculated as follows.

$$E(\%) = 1 - \frac{\tau_{DA}}{\tau_D}$$

E (%) represents the relative FRET efficiency, τ_{DA} the average weighted lifetime of donor in presence and τ_D in absence of the acceptor.

To elucidate whether obtained FRET values can be considered as a result of coclustering of raft marker and protein under study in lipid microdomains, or if they just reflect concentration depended random collision, the relation between acceptor concentration and FRET efficiency was examined. Confocal images were analyzed using ImageJ to obtain the fluorescence intensity of YFP at the plasma membrane assuming a direct proportion between acceptor concentration and fluorescence signal. Normalized and background corrected YFP fluorescence values were plotted against the

20

corresponding FRET efficiency for single observed cells and fitted to a binding kinetic model according to the following equation (Zacharias *et al.*, 2002).

$$E(\%) = \frac{E_{\max}(\%) \times F_{YFP}}{F_{YFP} + K_d}$$

Clustering in lipid rafts was assumed if obtained K_d values were significantly lower than the average acceptor fluorescence values F_{YFP} within the experiments (see Zacharias *et al.*, 2002; Scolari *et al.*, 2009 for more details).

Fluorescence polarization microscopy. The experimental setup for time resolved single photon detection was described above (FLIM-FRET imaging). An expanded setup explicitly described on the manufacturer website (Buschmann *et al.*, n.d.) was used for fluorescence anisotropy imaging. After removal of DIC depolarization filters, images were obtained with a 60x water objective (numerical aperture 1.2) with a frame size of 512x512 pixel. A pulsed 470 nm laser diode with a repetition frequency of 20 MHz was applied to excite YFP. The polarized emitted light was separated with a polarization beam splitter and parallel and perpendicular fluorescence signals were detected using a 540/40 emission filter for the perpendicular polarized light and a 540/30 emission filter for the parallel polarized light prior to a τ-SPAD and Perkin/Elmer SPAD respectively. The g-factor for this microscopic arrangement was calculated from point scans of the emission signals on both channels with an Alexa488 solution. Since the rotational correlation time of this dye is significantly higher than its average fluorescence lifetime the g-factor can be approximated by the quotient of parallel and perpendicular fluorescence intensity. A value of 0.73 was found for the setup described above. Fluorescence steady state anisotropy pictures were accumulated for 90 s with an average photon count rate of 50000-100000 counts per second. Images were analyzed using the SymPhoTime software after selection of suited regions of interest and obtained pixel weighted values were summed up into anisotropy histograms.

Statistical test. If not otherwise stated, experimental data represent the mean ± S.E. Statistical significance was assessed using the Student's t-Test with a 95% confidence interval and significance displayed as follows ***, $p < 0.001$; **, $p = 0.001-0.01$; *, $p = 0.01-0.05$.

Amino acid conservation analysis. If not otherwise stated, gp41 sequence conservation was examined for all available, complete sequences from HIV-1/SIVcpz from the Los Alamos HIV Sequence Database (http://www.hiv.lanl.gov) until 2012.

Classification of experimental results. To simplify the evaluation of the obtained data, the values were normalized according to the following equation and subsequently allocated to four different groups.

$$X = \frac{Mean - Mean_{Min}}{Mean_{Max} - Mean_{Min}}$$

With Mean representing the mean of the experimental data, $Mean_{Min}$ being the minimum and $Mean_{Max}$ being the maximum value of the respective assay. This normalization procedure allows a comparison of results from different experimental assays independent of the absolute values and the dynamic range of the individual method.

References:

Abad, C., Martínez-Gil, L., Tamborero, S., and Mingarro, I. (2009) Membrane topology of gp41 and amyloid precursor protein: interfering transmembrane interactions as potential targets for HIV and Alzheimer treatment. *Biochim Biophys Acta* **1788**: 2132–41

Aloia, R.C., Tian, H., and Jensen, F.C. (1993) Lipid composition and fluidity of the human immunodeficiency virus envelope and host cell plasma membranes. *Proc Natl Acad Sci U S A* **90**: 5181–5

Berlioz-Torrent, C., Shacklett, B.L., Erdtmann, L., Delamarre, L., Bouchaert, I., Sonigo, P., *et al.* (1999) Interactions of the cytoplasmic domains of human and simian retroviral transmembrane proteins with components of the clathrin adaptor complexes modulate intracellular and cell surface expression of envelope glycoproteins. *J Virol* **73**: 1350–61

Bernstein, H.B., Tucker, S.P., Kar, S.R., McPherson, S. a, McPherson, D.T., Dubay, J.W., *et al.* (1995) Oligomerization of the hydrophobic heptad repeat of gp41. *J Virol* **69**: 2745–50

Bhattacharya, J., Peters, P., and Clapham, P. (2004) immunodeficiency virus type 1 envelope glycoproteins that lack cytoplasmic domain cysteines: impact on association with membrane lipid rafts and incorporation onto. *J Virol* **78**: 5500–5506

Bhattacharya, J., Repik, A., and Clapham, P.R. (2006) Gag regulates association of human immunodeficiency virus type 1 envelope with detergent-resistant membranes. *J Virol* **80**: 5292–300

Borst, J.W., Willemse, M., Slijkhuis, R., Krogt, G. van der, Laptenok, S.P., Jalink, K., *et al.* (2010) ATP changes the fluorescence lifetime of cyan fluorescent protein via an interaction with His148. *PLoS One* **5**: e13862

Brügger, B., Glass, B., Haberkant, P., Leibrecht, I., Wieland, F.T., and Kräusslich, H.-G. (2006) The HIV lipidome: a raft with an unusual composition. *Proc Natl Acad Sci U S A* **103**: 2641–6

Buschmann, V., Bleckmann, A., Bülter, A., Krämer, B., Nikolaus, J., Roland, S., *et al.* Polarization Extension Unit for LSM Upgrade Kits q q. *pdfhttp://www.picoquant.com/images/uploads/page/files/7257/technote_polarization_extension_lsm.pdf* 1–7.

Byland, R., Vance, P.J., Hoxie, J.A., and Marsh, M. (2007) A conserved dileucine motif mediates clathrin and AP-2-dependent endocytosis of the HIV-1 envelope protein. *Mol Biol Cell* **18**: 414–25

Campbell, S., Gaus, K., Bittman, R., Jessup, W., Crowe, S., and Mak, J. (2004) The raft-promoting property of virion-associated cholesterol, but not the presence of virion-associated Brij 98 rafts, is a determinant of human immunodeficiency virus type 1 infectivity. *J Virol* **78**: 10556–65

Campbell, S., Oshima, M., Mirro, J., Nagashima, K., and Rein, A. (2002) Reversal by dithiothreitol treatment of the block in murine leukemia virus maturation induced by disulfide cross-linking. *J Virol* **76**: 10050–5

Campbell, S.M., Crowe, S.M., and Mak, J. (2002) Virion-associated cholesterol is critical for the maintenance of HIV-1 structure and infectivity. *AIDS* **16**: 2253–61

Center, R.J., Kemp, B.E., and Poumbourios, P. (1997) Human immunodeficiency virus type 1 and 2 envelope glycoproteins oligomerize through conserved sequences. *J Virol* **71**: 5706–11

Chan, W., Lin, H., and Chen, S. (2005) Wild-type-like viral replication potential of human immunodeficiency virus type 1 envelope mutants lacking palmitoylation signals. *J Virol* **79**: 8374–8387

Checkley, M.A., Luttge, B.G., and Freed, E.O. (2011) HIV-1 envelope glycoprotein biosynthesis, trafficking, and incorporation. *J Mol Biol* **410**: 582–608

Chen, S.S., Lee, S.F., and Wang, C.T. (2001) Cellular membrane-binding ability of the C-terminal cytoplasmic domain of human immunodeficiency virus type 1 envelope transmembrane protein gp41. *J Virol* **75**: 9925–38

Chen, S.S.-L., Yang, P., Ke, P.-Y., Li, H.-F., Chan, W.-E., Chang, D.-K., *et al.* (2009) Identification of the LWYIK motif located in the human immunodeficiency virus type 1 transmembrane gp41 protein as a distinct determinant for viral infection. *J Virol* **83**: 870–83

Day, J.R., Damme, N. Van, and Guatelli, J.C. (2006) The effect of the membrane-proximal tyrosine-based sorting signal of HIV-1 gp41 on viral infectivity depends on sequences within gp120. *Virology* **354**: 316–27

Dubay, J.W., Roberts, S.J., Hahn, B.H., and Hunter, E. (1992) Truncation of the human immunodeficiency virus type 1 transmembrane glycoprotein cytoplasmic domain blocks virus infectivity. *J Virol* **66**: 6616–25

Earl, P.L., Doms, R.W., and Moss, B. (1990) Oligomeric structure of the human immunodeficiency virus type 1 envelope glycoprotein. *Proc Natl Acad Sci U S A* **87**: 648–52

Earl, P.L., Koenig, S., and Moss, B. (1991) Biological and immunological properties of human immunodeficiency virus type 1 envelope glycoprotein: analysis of proteins with truncations and deletions expressed by recombinant vaccinia viruses. *J Virol* **65**: 31–41

Engel, S., Scolari, S., Thaa, B., Krebs, N., Korte, T., Herrmann, A., and Veit, M. (2010) FLIM-FRET and FRAP reveal association of influenza virus haemagglutinin with membrane rafts. *Biochem J* **425**: 567–73

Epand, R., and Thomas, A. (2006) Juxtamembrane protein segments that contribute to recruitment of cholesterol into domains. *Biochemistry* **45**: 6105–6114

Epand, R.M. (2008) Proteins and cholesterol-rich domains. *Biochim Biophys Acta* **1778**: 1576–82

Gao, F., Morrison, S.G., Robertson, D.L., Thornton, C.L., Craig, S., Karlsson, G., *et al.* (1996) Molecular cloning and analysis of functional envelope genes from human immunodeficiency virus type 1 sequence subtypes A through G. The WHO and NIAID Networks for HIV Isolation and Characterization. *J Virol* **70**: 1651–67

Graham, D.R.M., Chertova, E., Hilburn, J.M., Arthur, L.O., and Hildreth, J.E.K. (2003) Cholesterol Depletion of Human Immunodeficiency Virus Type 1 and Simian Immunodeficiency Virus with -

24

Cyclodextrin Inactivates and Permeabilizes the Virions: Evidence for Virion-Associated Lipid Rafts. *J Virol* **77**: 8237–8248

Guyader, M., Kiyokawa, E., Abrami, L., Turelli, P., and Trono, D. (2002) Role for human immunodeficiency virus type 1 membrane cholesterol in viral internalization. *J Virol* **76**: 10356–64

Hyun Bae, J., Rubini, M., Jung, G., Wiegand, G., Seifert, M.H.J., Azim, M.K., *et al.* (2003) Expansion of the Genetic Code Enables Design of a Novel "Gold" Class of Green Fluorescent Proteins. *J Mol Biol* **328**: 1071–1081

Keller, P., Toomre, D., Díaz, E., White, J., and Simons, K. (2001) Multicolour imaging of post-Golgi sorting and trafficking in live cells. *Nat Cell Biol* **3**: 140–9

Kellner, R.R., Baier, C.J., Willig, K.I., Hell, S.W., and Barrantes, F.J. (2007) Nanoscale organization of nicotinic acetylcholine receptors revealed by stimulated emission depletion microscopy. *Neuroscience* **144**: 135–43

Kim, J.H., Hartley, T.L., Curran, A.R., and Engelman, D.M. (2009) Molecular dynamics studies of the transmembrane domain of gp41 from HIV-1. *Biochim Biophys Acta* **1788**: 1804–12

Koga, Y., Sasaki, M., Yoshida, H., Oh-Tsu, M., Kimura, G., and Nomoto, K. (1991) Disturbance of nuclear transport of proteins in CD4+ cells expressing gp160 of human immunodeficiency virus. *J Virol* **65**: 5609–12

Lenz, O., Dittmar, M.T., Wagner, A., Ferko, B., Vorauer-Uhl, K., Stiegler, G., and Weissenhorn, W. (2005) Trimeric membrane-anchored gp41 inhibits HIV membrane fusion. *J Biol Chem* **280**: 4095–101

Levental, I., Grzybek, M., and Simons, K. (2010) Greasing their way: lipid modifications determine protein association with membrane rafts. *Biochemistry* **49**: 6305–16

Levental, I., Lingwood, D., Grzybek, M., Coskun, U., and Simons, K. (2010) Palmitoylation regulates raft affinity for the majority of integral raft proteins. *Proc Natl Acad Sci U S A* **107**: 22050–4

Liao, Z., Graham, D.R., and Hildreth, J.E.K. (2003) Lipid rafts and HIV pathogenesis: virion-associated cholesterol is required for fusion and infection of susceptible cells. *AIDS Res Hum Retroviruses* **19**: 675–87

Lichtenberg, D., Goñi, F.M., and Heerklotz, H. (2005) Detergent-resistant membranes should not be identified with membrane rafts. *Trends Biochem Sci* **30**: 430–6

Lifson, J.D., Reyes, G.R., McGrath, M.S., Stein, B.S., and Engleman, E.G. (1986) AIDS retrovirus induced cytopathology: giant cell formation and involvement of CD4 antigen. *Science* **232**: 1123–7

Linstedt, a D., Foguet, M., Renz, M., Seelig, H.P., Glick, B.S., and Hauri, H.P. (1995) A C-terminally-anchored Golgi protein is inserted into the endoplasmic reticulum and then transported to the Golgi apparatus. *Proc Natl Acad Sci U S A* **92**: 5102–5

Liu, J., Deng, Y., Li, Q., Dey, A.K., Moore, J.P., and Lu, M. (2010) Role of a putative gp41 dimerization domain in human immunodeficiency virus type 1 membrane fusion. *J Virol* **84**: 201–9

Liu, J., and Lu, M. (2010) Structure of the HIV-1 gp41 Membrane-Proximal Ectodomain Region in a Putative Prefusion Conformation. *Structure* **48**: 2915–2923.

Lopez-Vergès, S., Camus, G., Blot, G., Beauvoir, R., Benarous, R., and Berlioz-Torrent, C. (2006) Tail-interacting protein TIP47 is a connector between Gag and Env and is required for Env incorporation into HIV-1 virions. *Proc Natl Acad Sci U S A* **103**: 14947–52

Mañes, S., Real, G. del, Lacalle, R. a, Lucas, P., Gómez-Moutón, C., Sánchez-Palomino, S., *et al.* (2000) Membrane raft microdomains mediate lateral assemblies required for HIV-1 infection. *EMBO Rep* **1**: 190–6

McInerney, T.L., Ahmar, W. El, Kemp, B.E., and Poumbourios, P. (1998) Mutation-directed chemical cross-linking of human immunodeficiency virus type 1 gp41 oligomers. *J Virol* **72**: 1523–33

Mukherjee, S., Zha, X., Tabas, I., and Maxfield, F.R. (1998) Cholesterol distribution in living cells: fluorescence imaging using dehydroergosterol as a fluorescent cholesterol analog. *Biophys J* **75**: 1915–25

Muranyi, W., Malkusch, S., Müller, B., Heilemann, M., and Kräusslich, H.-G. (2013) Super-resolution microscopy reveals specific recruitment of HIV-1 envelope proteins to viral assembly sites dependent on the envelope C-terminal tail. *PLoS Pathog* **9**: e1003198

Nebl, T., Pestonjamasp, K.N., Leszyk, J.D., Crowley, J.L., Oh, S.W., and Luna, E.J. (2002) Proteomic analysis of a detergent-resistant membrane skeleton from neutrophil plasma membranes. *J Biol Chem* **277**: 43399–409

Nguyen, D.H., and Hildreth, J.E. (2000) Evidence for budding of human immunodeficiency virus type 1 selectively from glycolipid-enriched membrane lipid rafts. *J Virol* **74**: 3264–72

Ohno, H., Aguilar, R.C., Fournier, M.C., Hennecke, S., Cosson, P., and Bonifacino, J.S. (1997) Interaction of endocytic signals from the HIV-1 envelope glycoprotein complex with members of the adaptor medium chain family. *Virology* **238**: 305–15

Ohno, H., Fournier, M.-C., and Juan S. Bonifacino (1996) Structural Determinants of Interaction of Tyrosine-based Sorting Signals with the Adaptor Medium Chains. *J Biol Chem* **271**: 29009–29015

Ono, a, and Freed, E.O. (2001) Plasma membrane rafts play a critical role in HIV-1 assembly and release. *Proc Natl Acad Sci U S A* **98**: 13925–30

Owen, D.M., Magenau, A., Williamson, D., and Gaus, K. (2012) The lipid raft hypothesis revisited--new insights on raft composition and function from super-resolution fluorescence microscopy. *Bioessays* **34**: 739–47

Popik, W., Alce, T.M., and Au, W. (2002) Human Immunodeficiency Virus Type 1 Uses Lipid Raft-Colocalized CD4 and Chemokine Receptors for Productive Entry into CD4 Ƨ T Cells. *J Virol* **76**: 4709–4722.

Poumbourios, P., Ahmar, W. el, McPhee, D. a, and Kemp, B.E. (1995) Determinants of human immunodeficiency virus type 1 envelope glycoprotein oligomeric structure. *J Virol* **69**: 1209–18

Resh, M.D. (2004) Membrane targeting of lipid modified signal transduction proteins. *Subcell Biochem* **37**: 217–32

Resh, M.D. (2006) Palmitoylation of ligands, receptors, and intracellular signaling molecules. *Sci STKE* **2006**: re14

Rivinoja, A., Hassinen, A., Kokkonen, N., Kauppila, A., and Kellokumpu, S. (2009) Elevated Golgi pH impairs terminal N-glycosylation by inducing mislocalization of Golgi glycosyltransferases. *J Cell Physiol* **220**: 144–154

Rousso, I., Mixon, M.B., Chen, B.K., and Kim, P.S. (2000) Palmitoylation of the HIV-1 envelope glycoprotein is critical for viral infectivity. *Proc Natl Acad Sci U S A* **97**: 13523–5

Rowell, J.F., Stanhope, P.E., and Siliciano, R.F. (1995) Endocytosis of Endogenously Synthesized HIV-1 Envelope Protein. *J Immunol* **155**: 473–488

Roy, N.H., Chan, J., Lambelé, M., and Thali, M. (2013) Clustering and mobility of HIV-1 Env at viral assembly sites predict its propensity to induce cell-cell fusion. *J Virol* **87**: 7516–25

Salzwedel, K., West, J.T., and Hunter, E. (1999) A conserved tryptophan-rich motif in the membrane-proximal region of the human immunodeficiency virus type 1 gp41 ectodomain is important for Env-mediated fusion and virus infectivity. *J Virol* **73**: 2469–80

Sanchez, S. a, Tricerri, M. a, and Gratton, E. (2012) Laurdan generalized polarization fluctuations measures membrane packing micro-heterogeneity in vivo. *Proc Natl Acad Sci U S A* **109**: 7314–9

Schweizer, a, Fransen, J. a, Bächi, T., Ginsel, L., and Hauri, H.P. (1988) Identification, by a monoclonal antibody, of a 53-kD protein associated with a tubulo-vesicular compartment at the cis-side of the Golgi apparatus. *J Cell Biol* **107**: 1643–53

Scolari, S., Engel, S., Krebs, N., Plazzo, A.P., Almeida, R.F.M. De, Prieto, M., *et al.* (2009) Lateral distribution of the transmembrane domain of influenza virus hemagglutinin revealed by time-resolved fluorescence imaging. *J Biol Chem* **284**: 15708–16

Seifert, M.H.J., Ksiazek, D., Azim, M.K., Smialowski, P., Budisa, N., and Holak, T. a (2002) Slow exchange in the chromophore of a green fluorescent protein variant. *J Am Chem Soc* **124**: 7932–42

Sharma, P., Varma, R., Sarasij, R.C., Ira, Gousset, K., Krishnamoorthy, G., *et al.* (2004) Nanoscale organization of multiple GPI-anchored proteins in living cell membranes. *Cell* **116**: 577–89

Silvius, J.R. (2005) Partitioning of membrane molecules between raft and non-raft domains: insights from model-membrane studies. *Biochim Biophys Acta* **1746**: 193–202

Silvius, J.R., and Nabi, I.R. (2006) Fluorescence-quenching and resonance energy transfer studies of lipid microdomains in model and biological membranes. *Mol Membr Biol* **23**: 5–16

Simons, K., and Ikonen, E. (1997) Functional rafts in cell membranes. *Nature* **387**: 569–72

Simons, K., and Sampaio, J.L. (2011) Membrane organization and lipid rafts. *Cold Spring Harb Perspect Biol* **3**: a004697

Snijder, B., Sacher, R., Rämö, P., Damm, E.-M., Liberali, P., and Pelkmans, L. (2009) Population context determines cell-to-cell variability in endocytosis and virus infection. *Nature* **461**: 520–3

Sodroski, J., Goh, W.C., Rosen, C., Campbell, K., and Haseltine, W.A. (1986) Role of the HTLV-III/LAV envelope in syncytium formation and cytopathicity. *Nature* **322**: 470–474.

Somasundaran, M., and Robinson, H.L. (1987) A major mechanism of human immunodeficiency virus-induced cell killing does not involve cell fusion. *J Virol* **61**: 3114–9

Sugimoto, Y., Ninomiya, H., Ohsaki, Y., Higaki, K., Davies, J.P., Ioannou, Y. a, and Ohno, K. (2001) Accumulation of cholera toxin and GM1 ganglioside in the early endosome of Niemann-Pick C1-deficient cells. *Proc Natl Acad Sci U S A* **98**: 12391–6

Surma, M.A., Klose, C., and Simons, K. (2012) Lipid-dependent protein sorting at the trans-Golgi network. *Biochim Biophys Acta* **1821**: 1059–67

Thompson, R.J., Akana, H.C.S.R., Finnigan, C., Howell, K.E., and Caldwell, J.H. (2006) Anion channels transport ATP into the Golgi lumen. *Am J Physiol Cell Physiol* **290**: C499–514

Varma, R., and Mayor, S. (1998) GPI-anchored proteins are organized in submicron domains at the cell surface. *Nature* **394**: 798–801

Veillette, M., Désormeaux, A., Medjahed, H., Gharsallah, N.-E., Coutu, M., Baalwa, J., *et al.* (2013) Interaction with Cellular CD4 Exposes HIV-1 Envelope Epitopes Targeted by Antibody-Dependent Cell-Mediated Cytotoxicity. *J Virol*

Veit, M. (2012) Palmitoylation of virus proteins. *Biol Cell* **104**: 493–515

Vetrivel, K.S., Cheng, H., Lin, W., Sakurai, T., Li, T., Nukina, N., *et al.* (2004) Association of gamma-secretase with lipid rafts in post-Golgi and endosome membranes. *J Biol Chem* **279**: 44945–54

Villoing, A., Ridhoir, M., Cinquin, B., Erard, M., Alvarez, L., Vallverdu, G., *et al.* (2008) Complex fluorescence of the cyan fluorescent protein: comparisons with the H148D variant and consequences for quantitative cell imaging. *Biochemistry* **47**: 12483–92

Vincent, N., Genin, C., and Malvoisin, E. (2002) Identification of a conserved domain of the HIV-1 transmembrane protein gp41 which interacts with cholesteryl groups. *Biochim Biophys Acta* **1567**: 157–64

Wan, J., Roth, A.F., Bailey, A.O., and Davis, N.G. (2007) Palmitoylated proteins: purification and identification. *Nat Protoc* **2**: 1573–84

Wyatt, R., and Sodroski, J. (1998) The HIV-1 envelope glycoproteins: fusogens, antigens, and immunogens. *Science* **280**: 1884–8

Wyss, S., Berlioz-Torrent, C., Boge, M., Blot, G., Höning, S., Benarous, R., and Thali, M. (2001) The highly conserved C-terminal dileucine motif in the cytosolic domain of the human immunodeficiency virus type 1 envelope glycoprotein is critical for its association with the AP-1 clathrin adaptor [correction of adapter]. *J Virol* **75**: 2982–92

Yang, C., Spies, C.P., and Compans, R.W. (1995) The human and simian immunodeficiency virus envelope glycoprotein transmembrane subunits are palmitoylated. *Proc Natl Acad Sci U S A* **92**: 9871–5

Yang, P., Ai, L.-S., Huang, S.-C., Li, H.-F., Chan, W.-E., Chang, C.-W., *et al.* (2010) The cytoplasmic domain of human immunodeficiency virus type 1 transmembrane protein gp41 harbors lipid raft association determinants. *J Virol* **84**: 59–75

Yu, X., Yuan, X., McLane, M., Lee, T., and Essex, M. (1993) Mutations in the cytoplasmic domain of human immunodeficiency virus type 1 transmembrane protein impair the incorporation of Env proteins into mature virions. *J Virol* **19**: 505–10

Yuste, E., Johnson, W., Pavlakis, G.N., and Desrosiers, R.C. (2005) Virion envelope content, infectivity, and neutralization sensitivity of simian immunodeficiency virus. *J Virol* **79**: 12455–63

Zacharias, D. a, Violin, J.D., Newton, A.C., and Tsien, R.Y. (2002) Partitioning of lipid-modified monomeric GFPs into membrane microdomains of live cells. *Science* **296**: 913–6

Zheng, Y.H., Plemenitas, a, Linnemann, T., Fackler, O.T., and Peterlin, B.M. (2001) Nef increases infectivity of HIV via lipid rafts. *Curr Biol* **11**: 875–9.

Zheng, Y.-H., Plemenitas, A., Fielding, C.J., and Peterlin, B.M. (2003) Nef increases the synthesis of and transports cholesterol to lipid rafts and HIV-1 progeny virions. *Proc Natl Acad Sci U S A* **100**: 8460–5

Figure legends, tables:

Figure 1: Characterization of gp41 constructs. (A) Predicted structure of membrane adjacent domains of gp41. LLP1, LLP2, LLP3 are amphipathic α-helices supposed to interact with lipid bilayers. The Cholesterol Recognition Amino Acid Consensus, the known endocytosis motif 703YSPL706 and the palmitoylation cysteine at position 759 are in red. (B) Schematic representation of gp41 chimera with important motifs (see also A) in red. Membrane distant parts of the full gp160 wild type (gp160 wt) were replaced by a yellow fluorescent protein (YFP). Truncations and mutations (blue) were introduced yielding the variants gp41mCRAC, Δ1, Δ1mCRAC and Δ2 to study the influence of different domains on the protein properties. (C) Typical confocal images of CHO-K1 cells transfected with GPI-YFP or gp41 variants. Insets show a magnified region of the boxed area with red lines indicating the cell surface as deduced from DIC images. (D) The average YFP intensity at the plasma membrane of transfected CHO-K1 cells was obtained by analyzing background corrected confocal images. Each bar represents 20-50 cells from n independent experiments. (E) Living cells were labeled with anti-GFP antibodies. The fluorescence signal was detected as a measure of the plasma membrane expression of YFP-tagged proteins in flow cytometer experiments. The ratio of antibody fluorescence versus overall YFP fluorescence is displayed to determine the proportion of plasma membrane expression in relation to the total expression of YFP tagged proteins. Individual bars represent n independent experiments. In both graphs the error bars display SEM. *** $p<0.001$, ** $p=0.001-0.01$ and * $p=0.01-0.05$. (F) Acyl-biotinyl exchanged pulldown of gp41 fusion proteins. Isolated, palmitoylated proteins (palm) and the non-palmitoylated fraction (input) were detected on Western-blots using GFP antibodies. The protein gp41mPalm is a mutant of gp41-YFP (C764A).

Figure 2: Raft partitioning experiments using FLIM-FRET. (A) Typical confocal and FLIM images of a CHO-K1 cells transfected with the raft marker GPI-CFP and gp41-YFP. The pseudocolor scale of the FLIM image refers to the average lifetime in ns. The grey and white arrows indicate plasma membrane and perinuclear region, showing different CFP fluorescence lifetimes. (B) Results of a typical, single plasma membrane FLIM-FRET experiment including several control proteins. Fluorescence lifetime values of the FRET donor GPI-CFP were ascertained in presence and absence of gp41 acceptor proteins. The data represent the mean average lifetime in ns ± SEM of at least 10 cells per sample. (C) Plasma membrane FRET efficiencies with SEM calculated from n independent experiments each with 10-20 cells analyzed for all proteins under study. (D) Gp41-YFP expressing cells (green) were stained for Golgi apparatus proteins using fluorescent antibodies (purple). In the overlay image, colocalization appears in white. (E) FRET efficiencies with SEM in the Golgi apparatus from n independent experiments with 10 or more cells analyzed each. Statistical significance is shown as p<0.001 (***) and p=0.01-0.05 (*).

31

Figure 3: Analysis of raft clustering of gp41 variants. The FRET efficiencies of individual cells were plotted against their respective acceptor intensities to validate microdomain clustering. At least 20 cells of each construct were analyzed. FRET saturation fits (black lines) were generated according to the model previously published (1). (B) The FRET efficiencies of all cells showing raft related FRET (gp41, Δ1 and Δ2) were summarized in one histogram. Assuming two populations of cells with Gaussian distributions which possess different maximum FRET efficiencies of 18 and 6% yields a high FRET population containing 20% and a low FRET population covering the rest of the cells analyzed.

Figure 4: Oligomerization analysis using fluorescence polarization microscopy. (A) Fluorescence anisotropy images of CHO-K1 cells transfected with the raft marker GPI-YFP or gp41 constructs. The pseudocolor scale refers to the anisotropy in arbitrary units. (B) Individual cells were measured and an average anisotropy value from all detected proteins was calculated. Mean value of cells expressing GPI-YFP or gp41 variants from n independent experiments each with 5-15 cells per protein analyzed. (C) Oligomerization-localization analysis. Average anisotropy from plasma membrane (PM) and intracellular regions of 5-10 different cells from n independent experiments for gp41-YFP and Δ1 variant with SEM. *** p<0.001, ** p=0.001-0,01 and * p=0.01-0.05.

33

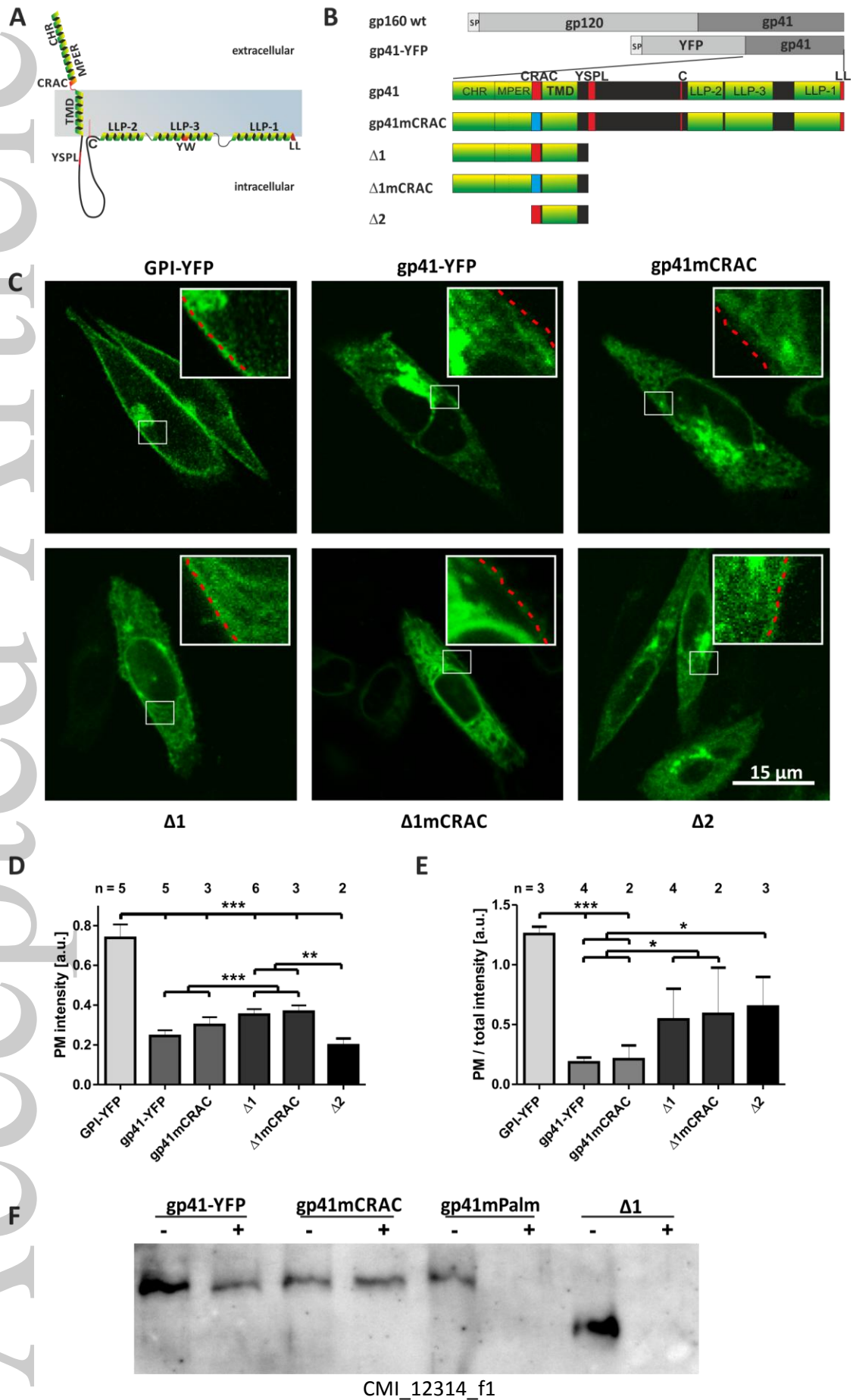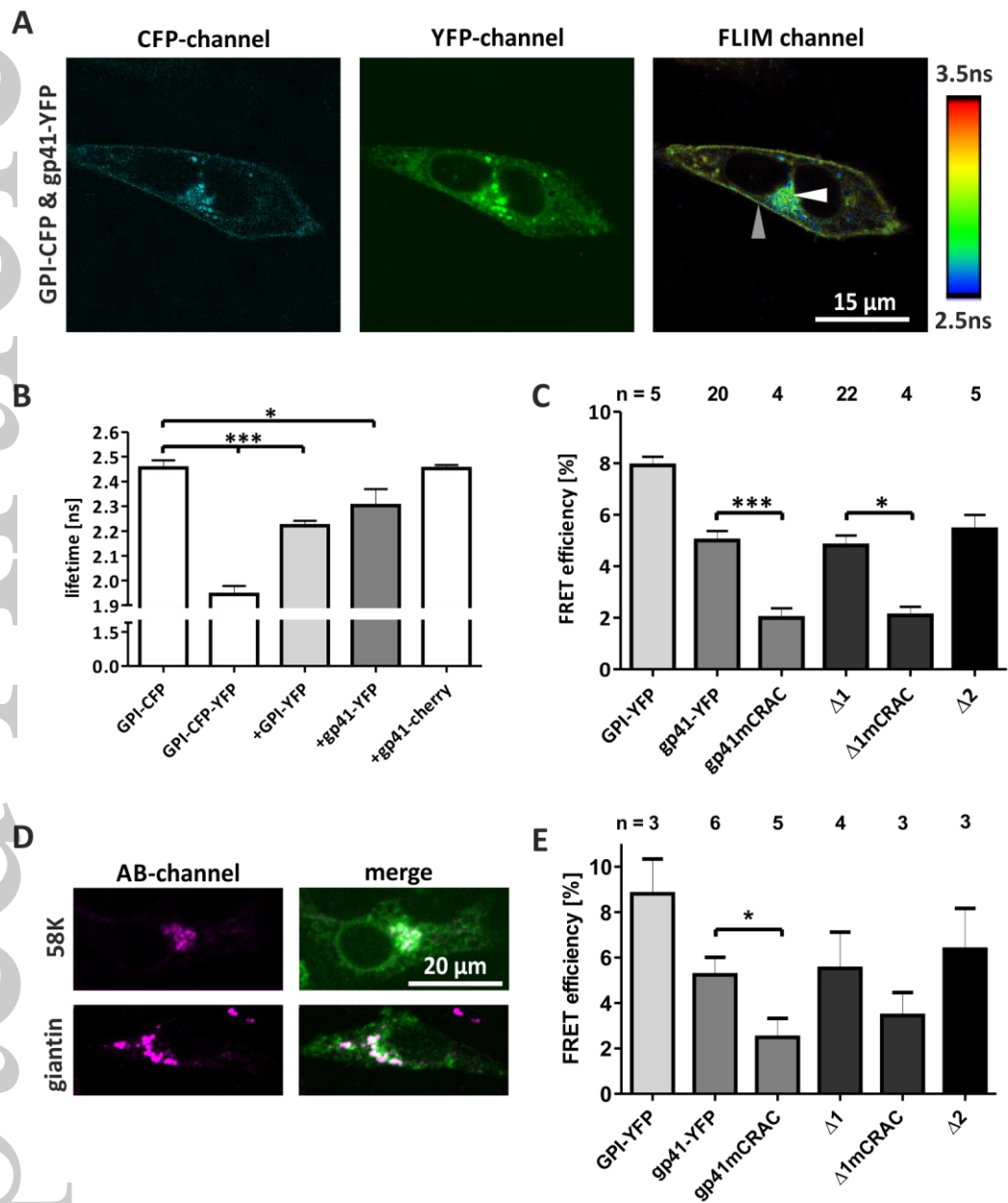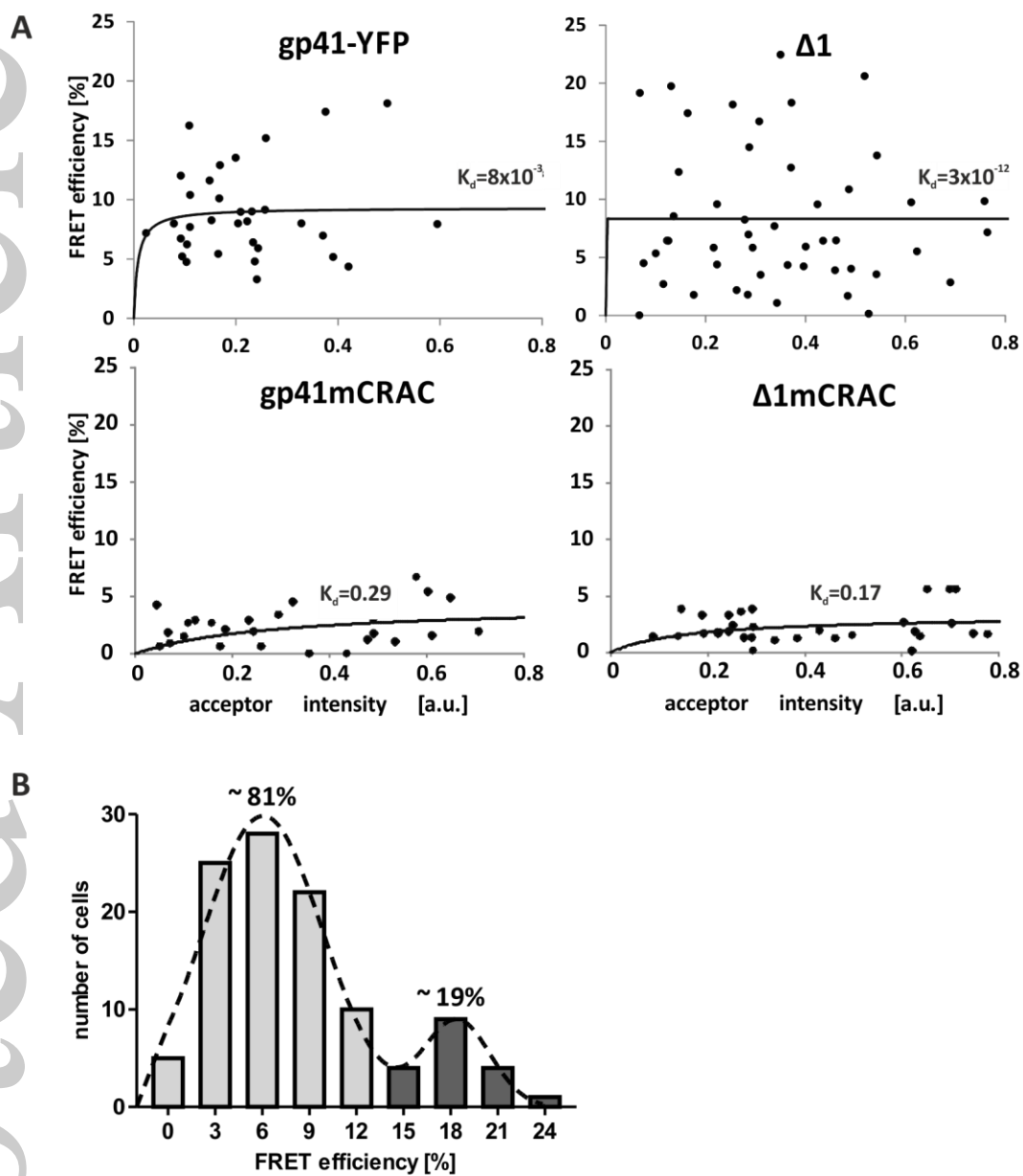|	GPI-YFP	Gp41-YFP	Gp41mCRAC	Δ1	Δ1mCRAC	Δ2
amino acids (HXB2 numeration)	/////	625-847	625-847	625-703	625-703	670-703
ratio PM to overall expression	+++	-	-	+	+	+
raft partitioning - PM	+++	+++	-	+++	-	+++
raft partitioning - Golgi	+++	++	-	+++	-	+++
oligomerization	-	+++	-	+++	-	-

Table 1: Summary of protein properties. The fluorescently labeled variants are compared with respect to the different protein properties studied. Values X in percentage of the maximum of the respective assay were normalized to the dynamic range of the collection of data and allocated to the following groups +++ : X<75%; ++ : 75 %<X<50% ; + : 50 %<X<25%; - : X<25%.
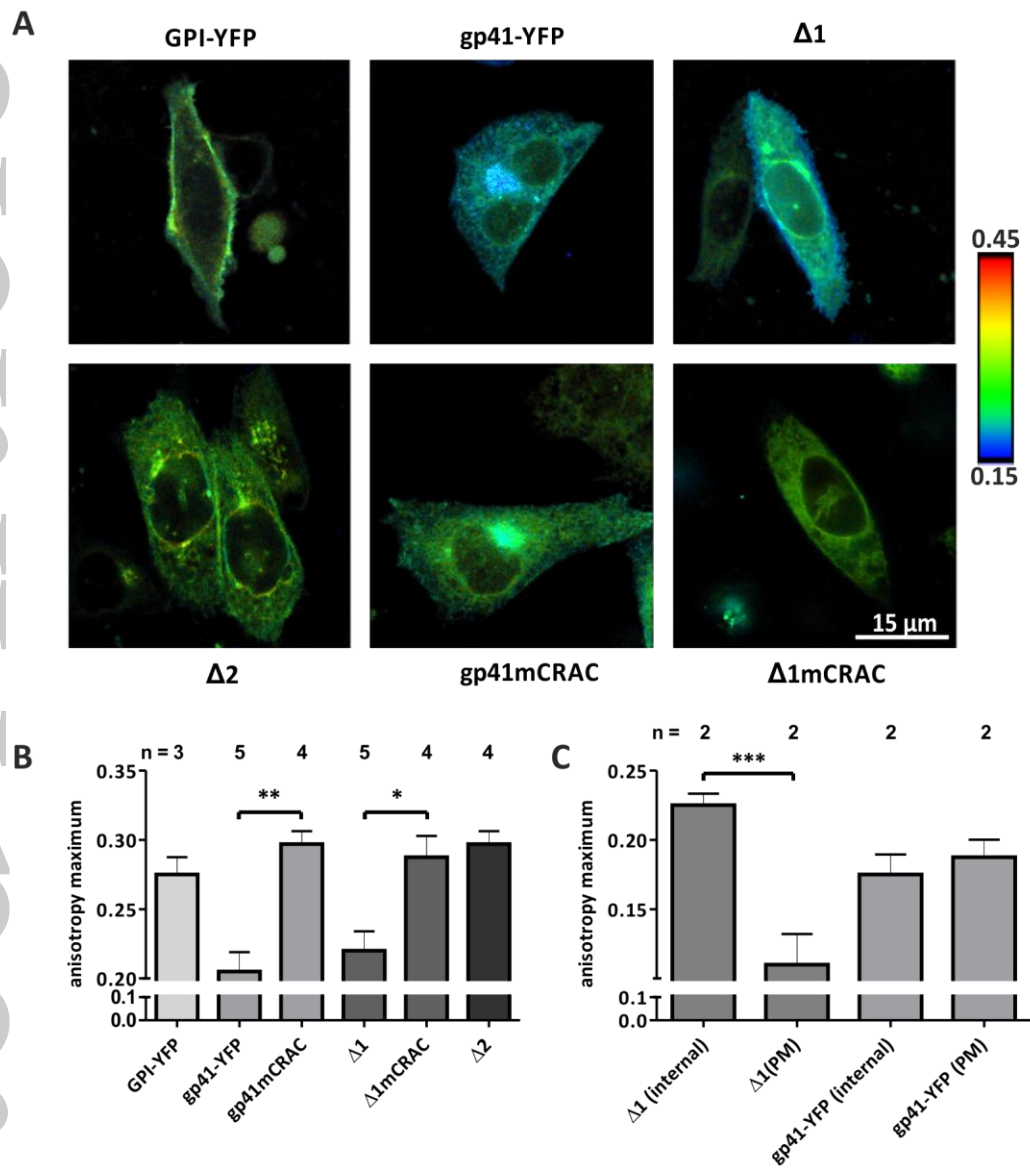
CMI_12314_f1

CMI_12314_f2

CMI_12314_f3

A

GPI-YFP gp41-YFP Δ1

0.45

0.15

Δ2 gp41mCRAC Δ1mCRAC

15 µm

B

anisotropy maximum

n = 3   5   4   5   4   4

**

*

GPI-YFP gp41-YFP gp41mCRAC Δ1 Δ1mCRAC Δ2

C

anisotropy maximum

n = 2   2   2   2

***

Δ1 (internal) Δ1(PM) gp41-YFP (internal) gp41-YFP (PM)

CMI_12314_f4

38